







Taking the Monte-Carlo gamble: How not to buckle under the pressure!

Yessica K. Gomez¹  | Andrew M. Natale¹  | James Lincoff¹  |
Charles W. Wolgemuth²  | John M. Rosenberg³  | Michael Grabe¹ 

¹Cardiovascular Research Institute, Department of Pharmaceutical Chemistry, University of California, San Francisco, San Francisco, California, USA

²Departments of Molecular and Cellular Biology and Physics, University of Arizona, Tucson, Arizona, USA

³Department of Biological Sciences, University of Pittsburgh, Pittsburgh, Pennsylvania, USA

Correspondence

Michael Grabe, Cardiovascular Research Institute, Department of Pharmaceutical Chemistry, University of California, San Francisco, San Francisco, CA, USA.
Email: michael.grabe@ucsf.edu

John M. Rosenberg, Department of Biological Sciences, University of Pittsburgh, Pittsburgh, PA, USA.
Email: jmr@pitt.edu

Charles W. Wolgemuth, Departments of Molecular and Cellular Biology and Physics, University of Arizona, Tucson, AZ, USA.
Email: wolg@arizona.edu

Funding information

National Institutes of Health, Grant/Award Numbers: 4T32HL007731-25, R01-GM117593, R01-GM089740, R01-GM137109; National Science Foundation, Grant/Award Number: 2034836

Abstract

Consistent buckling distortions of a large membrane patch ($200 \times 200 \text{ \AA}$) are observed during molecular dynamics (MD) simulations using the Monte-Carlo (MC) barostat in combination with a hard Lennard–Jones (LJ) cutoff. The buckling behavior is independent of both the simulation engine and the force field but requires the MC barostat-hard LJ cutoff combination. Similar simulations of a smaller patch ($90 \times 90 \text{ \AA}$) do not show buckling, but do show a small, systematic reduction in the surface area accompanied by $\sim 1 \text{ \AA}$ thickening suggestive of compression. We show that a mismatch in the way potentials and forces are handled in the dynamical equations versus the MC barostat results in a compressive load on the membrane. Moreover, a straightforward application of elasticity theory reveals that a minimal compression of the linear dimensions of the membrane, inversely proportional to the edge length, is required for buckling, explaining this differential behavior. We recommend always using LJ force or potential-switching when the MC barostat is employed to avoid undesirable membrane deformations.

KEYWORDS

barostat, curvature, lipid bilayer, molecular dynamics, Monte-Carlo

We observed consistent undesirable distortions of a membrane patch during molecular dynamics (MD) simulations in Amber18 using the Monte-Carlo (MC) barostat¹ in combination with a standard 10 \AA hard Lennard–Jones (LJ) cutoff as recently mentioned by Im and colleagues²; here we report our successful efforts to ameliorate this problem by employing force-switching (FS). The MC barostat, which is currently implemented in Amber and OpenMM, is a relatively new barostat that is frequently used for constant pressure simulations as it reproduces the correct volume fluctuations, unlike the Berendsen

barostat,³ and it does not require the virial to be computed at every time step, unlike most barostats.¹ Meanwhile, a 9 or 10 \AA hard cutoff for nonbonded interactions is commonly employed to improve simulation speed, as explicitly recommended for use with Amber force fields. When these parameters are used to simulate a $200 \times 200 \times 80 \text{ \AA}$ box, we observe significant rapid buckling of an initially flat membrane into an egg carton pattern that then breaks xy-symmetry to relax into a sinusoidal plane wave, as shown in Figure 1.

After this initial observation, we ran a series of test simulations using different MD engines to isolate which parameter combinations correlate with membrane distortions (Supplementary Table A1), comparing the MC algorithm with (1) the widely available but

Yessica K. Gomez, Andrew M. Natale, and James Lincoff have done equal contribution to this article.

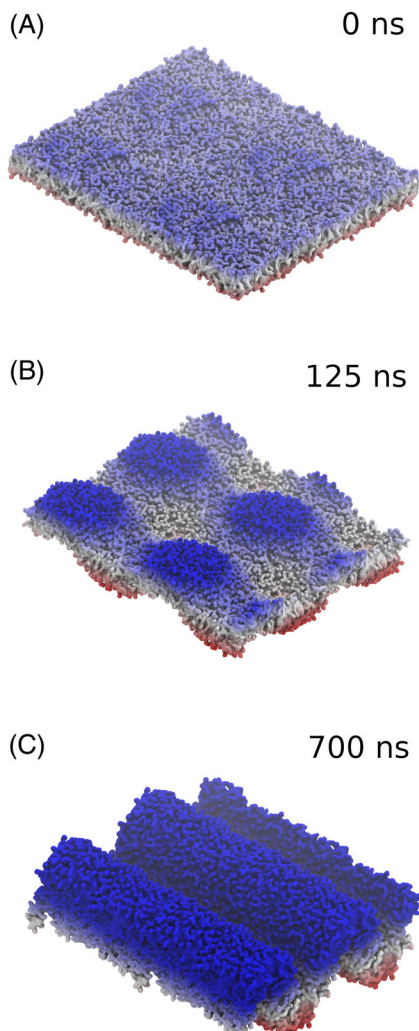


FIGURE 1 Membrane deformation induced by MC barostat and 10 Å cutoff. A 200 × 200 Å patch of POPC membrane with the hydrophobic lipid tails colored cyan and the head groups colored by height (z-coordinate—Blue positive, red negative). Note that all three panels show a 2 × 2 array of four simulation cells. (A) The initially flat membrane at the start of production exhibits minor height fluctuations. (B) By 125 ns, the membrane has buckled into an egg cartoon shape (see text). (C) By 700 ns, buckling has continued into nearly a steady state shape (see text)

problematic, Berendsen barostat and (2) the Parrinello-Rahman barostat⁴ implementation in Gromacs, which like the MC algorithm properly samples volume fluctuations. All simulations used semi-isotropic pressure scaling with coupling in the initial plane of the membrane (x–y plane) independent of the perpendicular axis. Examination of the box dimensions over time reveals that all simulations keep a constant volume (Supplementary Figure A1), albeit with up to 3% initial variation in the first few time steps in some cases; however, the MC barostat when used in combination with a 10 Å hard cutoff always results in a gradual compression of the x–y plane, and corresponding expansion along z, on the 100-ns time-scale (yellow traces in Figure 2A–C), leading to deformations like those shown in Figure 1.

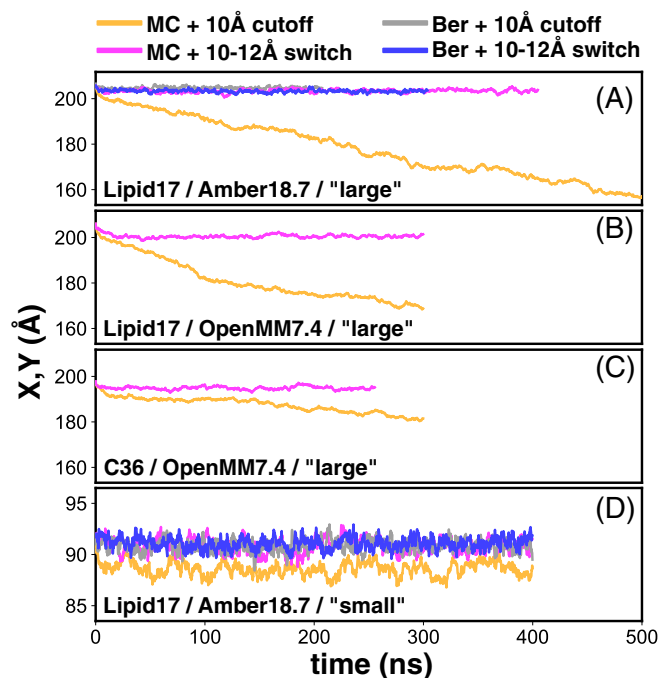


FIGURE 2 Changes in x/y-box dimensions over time for different combinations of system parameters. The identical length and width (x, y) of the membrane patches are plotted against time. The color key at the top defines combinations of barostats (MC-MC barostat or Ber-Berendsen) with LJ treatments (10 Å cutoff or 10–12 Å force switching). Each panel shows results for additional model combinations: (A) large membrane patch (initially 200 × 200 Å, Amber18.7 engine, and Lipid17 force field (#1–#4); (B) large patch, OpenMM7.4 engine, and Lipid17 (#9,#10); (C) large patch, OpenMM7.4 engine, and CHARMM36 force field (#11,#12); and (D) small patch (initially 90 × 90 Å, Amber18.7 engine, and Lipid17 (#15,#17,#18,#20). All numbers refer to simulations in Supplementary Information Table A1

Importantly, this phenomenon is not an artifact of a particular MD engine or force field as the buckling is reproduced in OpenMM as well as simulations performed with CHARMM36 (Supplementary Table A1), though CHARMM force fields are explicitly recommended for use with FS only. This suggests that the origin of the problem lies with the pairing of the MC barostat and a 10 Å (or shorter) LJ cutoff in membrane simulations. No other parameter combinations in Supplementary Table A1 resulted in significant membrane deformation.

We note that most published simulations employing the MC barostat in combination with a short LJ cutoff use smaller membrane patches, and they appear to be free of the distortions described above. We therefore tested whether 90 × 90 Å bilayers undergo buckling and found that they do not (Supplementary Table A1 and Supplementary Figure A1F). That said, the MC barostat simulation with 10 Å LJ cutoff does experience a 2 Å decrease of the x and y dimensions (yellow trace in Figure 2D) and a corresponding ~1 Å thickening of the width as if the membrane is under compression. Taken together, the extreme buckling observed on the large membrane patches coupled with the modest compression of the smaller patch suggests that there is an effective compressive force in the

membrane plane when the semi-isotropic MC barostat is used with a hard cutoff.

Changes to the LJ parameters are known to impact atomistic properties, including the particularly sensitive lipid density. Specifically, a hard LJ truncation of 10 Å reduces long range attraction compared to, say, a 10–12 Å switching distance, and might be expected to lead to a greater area-per-lipid (APL), as it does for the Berendsen barostat simulations (#3 and #4 in Supplementary Table A1). Why then does the MC barostat compress membranes when a short hard cutoff is employed? We believe that this arises from an inconsistency between the way forces and potentials are handled in the MC trial box-size change stage versus the dynamics stage. The MC barostat uses the potentials between pairs of atoms to determine whether a random box rescaling is energetically favorable. For a given configuration, atoms separated by a distance greater than the cutoff have zero interaction energy. However, in the dynamics steps, it is the force between atom pairs that is set to zero outside the cutoff distance, which is equivalent to a potential that is a negative constant for distances greater than the cutoff distance. These two corresponding LJ potential energy profiles are radically different (Supplemental Figure A2), with the MC barostat energy (potential U^2 in Supplemental Figure A2) containing an effective step change in the potential favoring smaller pairwise distances. This inconsistency between the assumed potentials in the MC and the MD steps leads to a discrepancy between the target equilibrium lipid densities in the bilayer, with a higher target density in the MC steps compared to the dynamics, introducing an effective compressive bias in the XY plane (see Supplementary Information Section 3).

We believe the problematic systems then evolve as follows. The flattened, effective potential employed during dynamics leads to lower in-plane lipid density by promoting out-of-plane lipid fluctuations resulting in membrane thickening. Meanwhile, the MC barostat favors higher in-plane lipid densities than the dynamics biasing volume trial moves toward compression of the xy-area over expansion. This area reduction exacerbates the crowding experienced during dynamics and the bilayer further thickens. This positive feedback cycle continues, eventually buckling the membrane. By using potential or force switching, even over very short distances, the target densities are consistent with one another, and the effective compression is removed so the membranes do not buckle (Supplementary Table A1, see simulation #9 vs. #25–27). Importantly, this process does not occur when a hard cutoff is employed with either the Berendsen or the Parrinello-Rahman barostats because they calculate the pressure from the virial, which uses MD forces—not energies—to drive changes in the box size based on the difference from the target pressure.

Next we employed an elastic energy model of the membrane that includes an energetic cost for in-plane compression together with a Helfrich-like bending energy⁵ to attempt to understand why small membranes only compress while large membranes buckle (see Supplementary Information Section 1 and Reference 6). According to this model, buckling occurs when the x/y cell dimensions decrease to the point where bending is more energetically favorable than in-plane

compression, giving a quantitative relationship for when that threshold is reached (Supplementary Information Equation (9)). When combined with the estimate of compressive strain induced by employing the MC barostat with a hard cutoff (Supplementary Information Equation (19)), we arrive at an expression that predicts the critical membrane length (L_{critical}) beyond which initially planar membrane patches of length (L_0) buckle:

$$L_0 > L_{\text{critical}} = \sqrt{\frac{\pi\kappa R^4}{4\rho_0^2\epsilon\lambda^6}} \propto R^2 \quad (1)$$

where κ is the bilayer bending modulus, ρ_0 is the initial lipid density (the inverse of the APL), ϵ and λ are the well depth and radius, respectively, of the LJ potential, and R is the applied LJ cutoff distance.

Putting this together, the compressive bias stresses the membrane, and that stress tends to grow with repetitive applications of the Metropolis algorithm until either the induced strain balances the effective compressive load or the membrane buckles. Compressive elastic balance is achieved quickly with the small ($L_0 = 90$ Å) membrane patch by a simple elastic compression. Equation (1) yields an L_{critical} value of 190 Å for a 10 Å hard LJ cutoff and the parameters of our simulations, correctly predicting that the small patch would not buckle while the 200 Å patch would. We conducted additional simulations to test these ideas (see Supplementary Information) including simulations with an 8 Å hard cutoff ($L_{\text{critical}} = 122$ Å) and a 12 Å hard cutoff ($L_{\text{critical}} = 274$ Å), and the results are all consistent with Equation (1). For example, a 200×200 Å patch with a 12 Å cutoff does not buckle, although it does show in-plane compression (#21 in Supplementary Table A1).

In conclusion, the extreme membrane distortions discussed here for the larger membrane patches only occur when using the MC barostat in combination with a 10 Å or less LJ cutoff; simply using a switching function avoids this undesirable result. While smaller patches do not undergo extreme distortion, they do deviate from experimentally derived parameters due to the effective compression; for instance, the APL shrinks from 68.7 ± 0.9 Å² to 65.7 ± 0.9 Å² when changing from a switching function to a hard cutoff (see #17 and #15 in Supplementary Information Table A1), with the former being in general agreement with the experimental value of 68.3 ± 1.5 Å^{2,7} but not the latter. These results raise a cautionary note regarding any membrane-containing simulation employing the MC barostat coupled with a hard LJ cutoff, and additional analysis would be needed to determine how other properties are impacted such as lipid-protein interactions or properties of mixed bilayers.

1 | METHODS

Initial atomic coordinates were generated using the CHARMM-GUI bilayer builder module.⁸ The “large” system contained 1200 POPC lipids, 53,866 water molecules with 0.15 M KCl, and had initial dimensions of $202 \times 202 \times 85$ Å³. The “small” system contained 240 POPC lipids, 10,766 water molecules with 0.15 M KCl and had initial dimensions of

$90 \times 90 \times 85 \text{ \AA}^3$. These structures were used to prepare all simulations. Two parameter sets were used in this study: (1) the Amber Lipid17⁹ force field with TIP3P water¹⁰ and Joung-Cheatham ions¹¹ (collectively referred to as “Lipid17” or “L17” throughout), or (2) the CHARMM36 lipid force field¹² with CHARMM TIP3P water¹⁰ and standard CHARMM ions (collectively referred to as “CHARMM36” or “C36” throughout).

From the starting coordinates, we initiated five separate equilibration runs: (a) “large” system with the Lipid17 forcefield in the Amber engine¹³; (b) “large” system with the CHARMM36 forcefield in the Amber engine; (c) “large” system with the CHARMM36 forcefield in the OpenMM engine¹⁴; (d) “large” system with the CHARMM36 forcefield in the Gromacs engine¹⁵; and (e) “small” system with the Lipid17 forcefield in the Amber engine. Heavy atoms were restrained with a force constant of $1.0 \text{ kcal/mol/\AA}^2$, and restraints were eased stepwise over 125 ps, followed by 20 ns of unrestrained dynamics. During equilibration, treatment of Van der Waals forces was done according to what is considered standard for the force field, that is, for CHARMM36 Lennard-Jones (LJ) forces were switched smoothly to zero in the range 10–12 Å, while for Lipid17 a plain cutoff of 10 Å was used. For equilibration of all simulations, a Berendsen barostat was used. All equilibration and production simulations used semi-isotropic pressure coupling requiring the x and y dimensions of the simulation cell to scale together while z scaled freely, a target pressure of 1 atm, a 2 fs timestep, and in all cases, long range electrostatic interactions were treated using the Particle Mesh Ewald method.¹⁶ Water molecules were kept rigid using the SETTLE algorithm,¹⁷ and bonds to hydrogen atoms were converted to rigid constraints using either the SHAKE¹⁸ (Amber and OpenMM) or LINCS¹⁹ (Gromacs) algorithms. All simulations in Amber and OpenMM used a Langevin thermostat with a friction coefficient of 1 ps^{-1} , while those in Gromacs used a Berendsen thermostat during equilibration and thereafter a Nose-Hoover thermostat. In all cases temperature was maintained at 310 K. Simulations using a MC barostat applied trial moves to the box vectors once per every 100 dynamics steps.

Each of the five equilibrated systems (coordinates, velocities, and box vectors) was used as the common starting point for several production trajectories with different settings and parameters outlined in Supplementary Table A1 and here in the main text.

ACKNOWLEDGMENTS

We would like to thank William DeGrado for first noticing the initial distortions and prompting us to explore the cause. This work was supported by a National Science Foundation Graduate Research Fellowship (YKG) and National Institutes of Health grants R01-GM089740, R01-GM117593, R01-GM137109, and Postdoctoral fellowship 4T32HL007731-25 (JL).

DATA AVAILABILITY STATEMENT

The data that support the findings of this study are available from the corresponding author(s) upon reasonable request.

ORCID

Yessica K. Gomez  <https://orcid.org/0000-0002-3976-5209>

Andrew M. Natale  <https://orcid.org/0000-0002-6320-0216>

James Lincoff  <https://orcid.org/0000-0003-3090-1240>

Charles W. Wolgemuth  <https://orcid.org/0000-0002-3588-3136>

John M. Rosenberg  <https://orcid.org/0000-0001-7616-4376>

Michael Grabe  <https://orcid.org/0000-0003-3509-5997>

REFERENCES

- [1] J. Åqvist, P. Wennerström, M. Nervall, S. Bjelic, B. O. Brandsdal, *Chem. Phys. Lett.* **2004**, 384(4–6), 288.
- [2] J. Lee, M. Hitznerberger, M. Rieger, N. R. Kern, M. Zacharias, W. Im, *J. Chem. Phys.* **2020**, 153(3), 035103.
- [3] H. J. Berendsen; J. Postma, W.F. van Gunsteren; A DiNola, J. R Haak. *J. Chem. Phys.* **1984**, 81(8), 3684–3690.
- [4] M. Parrinello, A. Rahman, *J. Appl. Phys.* **1981**, 52(12), 7182.
- [5] W. Helfrich, *Z. Naturforsch [C]* **1973**, 28(11), 693.
- [6] J. Eid, H. Razmazma, A. Jraj, A. Ebrahimi, L. Monticelli, *J. Phys. Chem. B* **2020**, 124(29), 6299.
- [7] N. Kučerka, S. Tristram-Nagle, J. F. Nagle, *J. Membrane Biol.* **2006**, 208(3), 193.
- [8] J. Lee, X. Cheng, J. M. Swails, M. S. Yeom, P. K. Eastman, J. A. Lemkul, S. Wei, J. Buckner, J. C. Jeong, Y. Qi, S. Jo, V. S. Pande, D. A. Case, C. L. Brooks, A. D. MacKerell, Jr., J. B. Klauda, W. Im, *J. Chem. Theory Comput.* **2016**, 12(1), 405–413.
- [9] C. J. Dickson, B. D. Madej, A. A. Skjevik, R. M. Betz, K. Teigen, I. R. Gould, R. C. Walker, *J. Chem. Theory Comput.* **2014**, 10(2), 865.
- [10] W. L. Jorgensen, J. Chandrasekhar, J. D. Madura, R. W. Impey, M. L. Klein, *J. Chem. Phys.* **1983**, 79(2), 926.
- [11] I. S. Joung, T. E. Cheatham, *J. Phys. Chem. B* **2008**, 112(30), 9020.
- [12] J. B. Klauda, R. M. Venable, J. A. Freites, J. W. O'Connor, D. J. Tobias, C. Mondragon-Ramirez, I. Vorobyov, A. D. MacKerell, R. W. Pastor, *J. Phys. Chem. B* **2010**, 114(23), 7830.
- [13] D. A. Case, (University of California, San Francisco, **2015**).
- [14] P. Eastman, J. Swails, J. D. Chodera, R. T. McGibbon, Y. Zhao, K. A. Beauchamp, L. P. Wang, A. C. Simmonett, M. P. Harrigan, C. D. Stern, R. P. Wiewiora, B. R. Brooks, V. S. Pande, *PLoS Comput. Biol.* **2017**, 13(7), e1005659.
- [15] M. J. Abraham, T. Murtola, R. Schulz, S. Páll, J. C. Smith, B. Hess, E. Lindahl, *SoftwareX* **2015**, 1, 19.
- [16] T. Darden, D. York, L. Pedersen, *J. Chem. Phys.* **1993**, 98(12), 10089.
- [17] S. Miyamoto, P. A. Kollman, *J. Comput. Chem.* **1992**, 13(8), 952.
- [18] J. P. Ryckaert, G. Ciccotti, H. J. C. Berendsen, *J. Comp. Phys.* **1977**, 23, 327.
- [19] B. Hess, H. Bekker, H. J. C. Berendsen, J. G. E. M. Fraaije, *J. Comput. Chem.* **1997**, 18(12), 1463.

SUPPORTING INFORMATION

Additional supporting information may be found in the online version of the article at the publisher's website.

How to cite this article: Y. K. Gomez, A. M. Natale, J. Lincoff, C. W. Wolgemuth, J. M. Rosenberg, M. Grabe, *J. Comput. Chem.* **2022**, 43(6), 431. <https://doi.org/10.1002/jcc.26798>